Enabling Interplanetary Exploration for CubeSats with a Fully Chemical Propulsion System

Giordano, A.; Cervone, A.

DOI
10.59332/jbis-076-04-0134

Publication date
2023

Document Version
Final published version

Published in
JBIS - Journal of the British Interplanetary Society

Enabling Interplanetary Exploration for CubeSats with a Fully Chemical Propulsion System

A. GIORDANO, A. CERVONE Department of Space Engineering, Faculty of Aerospace Engineering, Technische Universiteit Delft, 2628 CD Delft, Netherlands

Email antonio.giordano996@gmail.com

DOI https://doi.org/10.59332/jbis-076-04-0134

Interplanetary CubeSat missions are currently becoming more popular, with a significant number of recently planned missions. The context of this paper is a Mars mission, starting from a parking orbit around Earth: the adoption of a chemical propulsion system for the Earth-Mars transfer phase is investigated, considering the recent technological developments for CubeSats. A trade-off of propulsion system type and propellant results in the choice of a mono-propellant system adopting the HAN-based propellant AF-M315E (ASCENT). The main challenge for the propulsion system is to fit inside a CubeSat standardised volume, which can range up to 24 U, for which the implementation of a suitable COTS micro-pump is considered. Finally, the complete architecture and design of the propulsion system is presented. This work demonstrates the feasibility of adopting full chemical propulsion for an interplanetary CubeSat mission, with consequent advantages in terms of transfer time and required power, at the cost of relatively small mass and volume left for the other subsystems. Even better results can be expected for interplanetary missions requiring slightly lower ΔV budgets, such as Near Earth Objects exploration or asteroid fly-by missions.

Keywords: CubeSat, Chemical Propulsion, Green Mono-propellant, Interplanetary Mission, Mars Exploration

1 INTRODUCTION

CubeSats applications are receiving growing interest from universities, companies and space agencies for their high potential of producing scientific data while being considerably less expensive, both economically and in terms of development time, when compared to bigger satellites. During the contemporary era of "New-space", CubeSats missions have concentrated towards Low Earth Orbit (LEO) applications, but CubeSat missions increasing the range of scientific results that can be achieved with smaller satellites are being investigated. The MarCO mission, developed by JPL and launched in 2018, included two 6U CubeSats that performed a fly-by near Mars in order to provide communication relay to the descending InSight Mars [1]: up to now, it is the only interplanetary CubeSat mission ever launched. Another example of a CubeSat mission that extends its horizon beyond Earth applications adopting its own propulsion system, is LUMIO (LUnar Meteoroid Impact) [2]: it comprises of a 12U CubeSat equipped with an optical payload that will use its main propulsion system to reach an Earth-Moon L2 halo orbit for its operations, currently in development by an international consortium led by Politecnico di Milano.

It is envisioned that in the future fast deep-space cruising might be achievable by employing CubeSats that are able to propel themselves with their own propulsion system, exiting Earth's sphere of influence and reaching other celestial objects. In order to do this, it is crucial to adopt a propulsion system capable of providing high thrust levels to the spacecraft to start its interplanetary voyage: this will lead to lower transfer times and will also reduce the impact of radiation

NOMENCLATURE & ABBREVIATIONS

a	Orbit semi-major axis
e	Orbit eccentricity
θ	Orbit true anomaly
μ	Gravitational parameter
I_{sp}	Specific impulse
ρI_{sp}	Volumetric specific impulse
t_{burn}	Thruster burning time
Δt_{burn}	Waiting time in between maneuvers
ΔV	Delta-V
ADN	Ammonium DiNitramide
HAN	HydroxylAmmonium Nitrate
AF-M315E	Air Force Mono-propellant 315E
COTS	Commercial Off-The-Shelf
GPIM	Green Propellant Infusion Mission
RPA	Rocket Propulsion Analysis
SOI	Sphere Of Influence
SSGTO	Super Synchronous Geostationary Transfer Orbit
TRL	Technology Readiness Level

This paper was first presented at the 73rd International Astronautical Congress (IAC), Paris, France, 18-22 September 2022.
Paper No. IAC-22.C4.9.9

onto the spacecraft caused by Van Allen belts crossings. Following this concept, the MARIO mission (Mars Atmospheric Radiation Imaging Orbiter) proposes to adopt two separate chemical and electric propulsion systems on-board of a 16U CubeSat, achieving Earth escape and transfer to Mars, with the objective of conducting thermal radiation imaging of the thermal environment in the Mars upper atmosphere [3]. The MARIO mission is taken as a baseline to analyse the feasibility of performing an interplanetary transfer between Earth and Mars, achieving all orbital transfers by adopting a single chemical propulsion system. This feasibility study has the objective of gauging the improvements that chemical propulsion systems for CubeSats can provide to small satellite mission horizons.

2 MISSION CHARACTERISTICS AND REQUIREMENTS

An interplanetary mission from Earth to Mars is envisioned to require a ΔV budget in the orders of km/s, which when adopting a chemical propulsion system places a burden on the amount of available mass and volume left to the rest of the subsystems and payloads: for this reason, the CubeSat volume units for the mission are allowed to be up to 24 U, composed by two 12 U CubeSats stacked on top of each other.

2.1 Mission requirements

As a first stepping stone towards the definition of an Earth to Mars mission, a set of preliminary mission requirements is chosen. The starting orbit is the Super Synchronous Geostationary Transfer Orbit (SSGTO) taken as reference from the MARIO mission, which is defined by Keplerian semi-major axis and eccentricity: {a,e} = {51,526 km, 0.8705}. Falcon 9 rocket launched Thaicom 6 into this orbit in January 2014 [4]. From this parking orbit, the spacecraft shall perform orbit raising manoeuvres until it reaches a high specific energy of the orbit that allows for an interplanetary transfer to Mars. The first requirement, MISS-E01, is set based on the number of orbit raising manoeuvres performed in the MARIO mission in order to achieve Earth escape, minimizing the Van Allen belt crossings [3]. The second requirement, MISS-E02, comes from the preliminary mission analysis which is described in the next section and sets a minimum value of orbit specific energy to perform the interplanetary transfer. While at this stage of feasibility study no actual payload has been defined, it is envisioned that this mission could be adopted for optical payloads: this would require close and frequent passages near the surface of Mars, requiring a minimum distance from the planet to generate scientific data. To constrain the final operational orbit, the values of orbit eccentricity and periapsis height have been fixed in MISS-M01 and MISS-M02. The complete set of mission requirements is highlighted in Table 1.

2.2 Propulsion system requirements

The requirements that the chemical propulsion system shall comply to are related to its performance levels and greenness. The first parameter to be defined is the ΔV budget, leading to requirement PROP-01, which will determine the amount of propellant to be carried on board: an estimate of this value can be obtained by the assumption of instantaneous manoeuvres, but a more precise estimation based on the limitations of CubeSat propulsion system performance parameters is obtained in the next chapter by means of analysis. An important parameter to be defined is the thrust level, which is constrained to be at most double the maximum allowable level for MARIO, since it is expected that a higher level of thrust is needed from the chemical propulsion system to correctly perform the interplanetary transfer on its own: this determines requirement PROP-02. The maximum continuous thrusting time (or burn time, t_{burn}) is fixed based on the same requirement from MARIO, minimizing gravity losses [3], for requirement PROP-03. Finally, the adoption of non-toxic green propellant is considered, leading to requirement PROP-04. These considerations lead to the definition of four propulsion system requirements, summarized in Table 2.

3 PRELIMINARY ΔV ANALYSIS

The estimation of ΔV highlighted in PROP-01 has been obtained by using the patched-conics method applied to an interplanetary Hohmann transfer between Earth and Mars. Taking into consideration all mission and propulsion system requirements, with other additional constraints described in the following sections, the optimal value of ΔV budget that satisfies the requirements, present in PROP-01, has been obtained.

3.1 Interplanetary flight assumptions

The patched-conics method allows for an early estimate of time and required ΔV needed for the three phases of the interplanetary flight. The three phases are:

1. A first phase of manoeuvres performed around Earth,

TABLE 1: Mission Requirements

ID	Requirement
MISS-E01	The number of orbit raising manoeuvres around Earth shall be at most 6
MISS-E02	The specific energy of the orbit before leaving Earth's sphere of influence shall be at least 4.332 km^2/s^2
MISS-M01	The final orbit eccentricity after stabilization shall be less than 0.92.
MISS-M02	The periapsis height of the Mars operational orbit shall be less than 2,000 km

TABLE 2: Propulsion Requirements

ID	Requirement
PROP-01	The chemical propulsion system shall provide at least a ΔV budget of 2,046.34 m/s
PROP-02	The maximum thrust level of the system shall be at most 6 N
PROP-03	The maximum burn time t_{burn} shall be at most 600 s for each time the propulsion system is activated
PROP-04	The propulsion system shall utilize non-toxic "green" propellant

transforming the elliptic parking orbit into a hyperbolic orbit. The final hyperbolic orbit shall be characterized by an "infinite velocity" $v_{\infty E}$ that summed up with the one of the Earth around the Sun, allows for an Hohmann transfer between Earth and Mars.
2. The trajectory of the interplanetary flight around the Sun is assumed to be an elliptic Hohmann transfer between Earth and Mars, within the sphere of influence of the Sun.
3. A final braking manoeuvre phase: once the Hohmann transfer is completed, the spacecraft enters the sphere of influence of Mars with relative velocity $v_{\infty M}$ and shall reduce its orbital velocity to change the shape of its trajectory around Mars from a hyperbolic orbit to an elliptic orbit.

Assuming circular and co-planar orbits of Earth and Mars around the Sun, the values of specific orbit energy associated with these infinite velocities are found in $E_{\infty E}$ = 4.332 km^2/s^2 and $E_{\infty M}$ = 3.5057 km^2/s^2. If the value of specific orbit energy $E_{\infty E}$ is reached during the Earth escape phase, the interplanetary transfer can be approximated with an Hohmann transfer and the sphere of influence of Mars is reached with a hyperbolic orbit characterized by the specific orbit energy value of $E_{\infty M}$.

3.2 Earth escape strategy

The phase of Earth escape is obtained by sequentially performing manoeuvres to raise the energy of the orbit, until reaching the value of $E_{\infty E}$. The spacecraft will experience two phases of Earth escape:
1. Orbit raising, in which the energy of the orbit increases after each manoeuvre but remains below 0, keeping the orbit elliptical.
2. Hyperbolic phase, in which its trajectory has become hyperbolic, but the thrusters still need to be activated to increase the energy of the orbit up to the value of $E_{\infty E}$.

The trajectory of the spacecraft is simulated by solving the orbital equation of motion of a two-body problem around Earth, described by Equation (1):

$$\ddot{\vec{r}} = -\frac{\mu_E}{\left|\left|\vec{r}\right|\right|^3}\vec{r} + \frac{\vec{T}}{m} \tag{1}$$

The vector $\vec{r}$ represents the position of the spacecraft, thrust is represented with the vector $\vec{T}$ and is assumed to be aligned with the orbital velocity (when a manoeuvre is performed) and m is the current spacecraft mass. During the first phase of Earth escape, the manoeuvres are performed only around the perigee of the orbit. The orbit true anomaly at which each manoeuvre is started, is found through Equations (2)-(3):

$$E_{man\_E} - e\,sinE_{man\_E} = \sqrt{\frac{\mu_e}{a^3}} \cdot \frac{t_{burn}}{2} \tag{2}$$

$$\theta_{man\_E} = 2\,arctan\left[\sqrt{\frac{1+e}{1-e}}tan\left(\frac{E_{man\_E}}{2}\right)\right] \tag{3}$$

By adopting Equations (2) and (3), an optimal value of true anomaly θ_{man_E} at which to start the manoeuvre is found for each orbit raising, by means of the eccentric anomaly E_{man_E}. Thrust is applied symmetrically for half of the burn time duration before the perigee and for the other half after the perigee, minimizing gravity losses.

Once the orbit energy becomes positive and the trajectory is hyperbolic, the second phase of Earth escape begins, in which manoeuvres still need to be performed in order to reach the adequate level of $E_{\infty E}$. This is implemented by assuming that manoeuvres shall still last t_{burn}, with a waiting time of $\Delta t_{burn} = t_{burn}$ each, until the orbit specific energy reaches the value of $E_{\infty E}$.

Two constraints have been imposed to the Earth escape phase: the first one is related to the total time spent around Earth with a closed orbit from the beginning of the Earth escape phase, which has been limited to be below 1,000 h. A longer residence time would mean that the spacecraft will pass several times through the Van Allen belts, increasing the risk of electronics malfunction due to high levels of ionizing dose. The second constraint is related to the maximum distance from Earth, which is imposed to be lower than a factor 0.9 of the radius of Earth's sphere of influence. The sphere of influence concept is crucial in this simulation since it defines the ideal volume in which the satellite motion can be described as a two-body problem without the effect of additional celestial objects.

By varying the available thrust and burn time, the amount of ΔV required can be estimated. Figure 1 shows the results obtained for an initial spacecraft mass of 28 kg, with specific impulse of 262.86 s: these values are obtained after the overall optimization of the mission for the initial spacecraft mass and propulsion system specific impulse. The thrust level has been varied between 4 to 6 N, while the manoeuvre burn time t_{burn} is varied between 400 to 600 s for each case.

In blue, the combination of T-t_{burn} for which the requirement of specific orbit energy, or one of the imposed constraints, are not satisfied. The optimal value is found for a thrust level of 6 N and single burn time of t_{burn} = 465.3 s, amounting to a ΔV budget for this phase of 903.68 m/s. Table 3 shows the complete set of results. Figure 2 shows the trajectory followed by the spacecraft during the Earth escape phase. The number of orbit-raising manoeuvres is 4; the number of Van Allen Belt crossings amounts to 9.

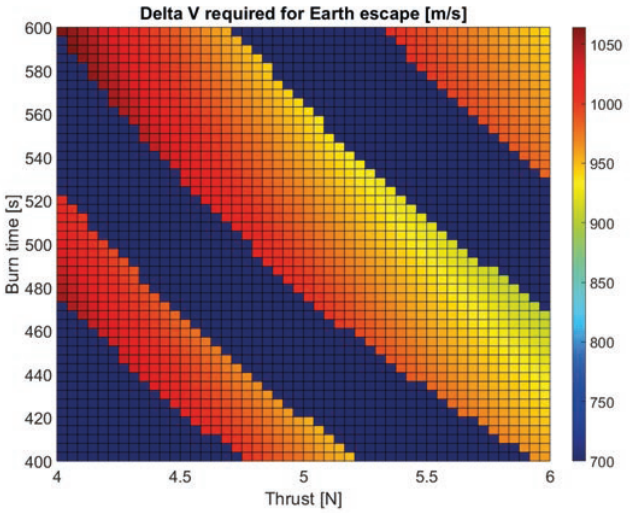

Fig.1 ΔV **budget for Earth escape phase.**

TABLE 3: Earth escape phase results

Property	Value	Unit
Initial spacecraft mass	28	kg
Thrust	6	N
Specific impulse	262.86	s
Manoeuvre burn time t_{burn}	465.3	s
Orbit raising manoeuvres	4	-
Manoeuvres along hyperbola	4	-
Total burn time	3,557.5	s
ΔV – Earth escape	903.68	m/s
Propellant mass used	8.2775	kg
Final mass at Earth escape	19.722	kg
Final specific orbit energy	4.3322	km²/s²
Time to reach Earth's SOI	991	h

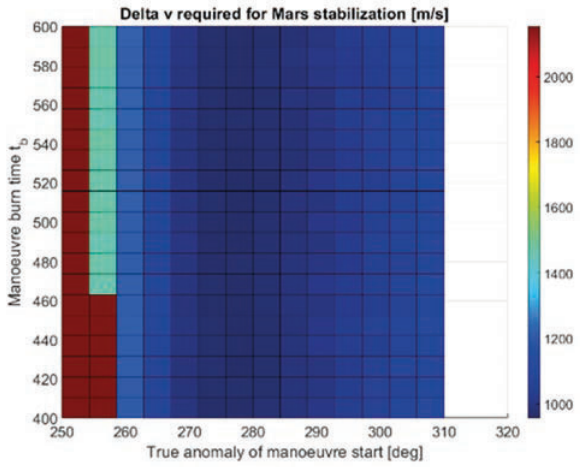

Fig.3 ΔV **budget for Mars stabilization.**

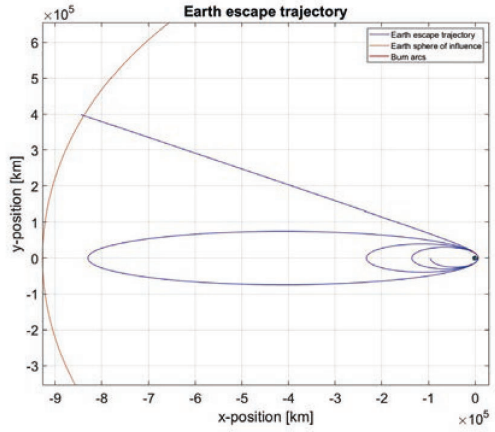

Fig.2 Earth escape trajectory.

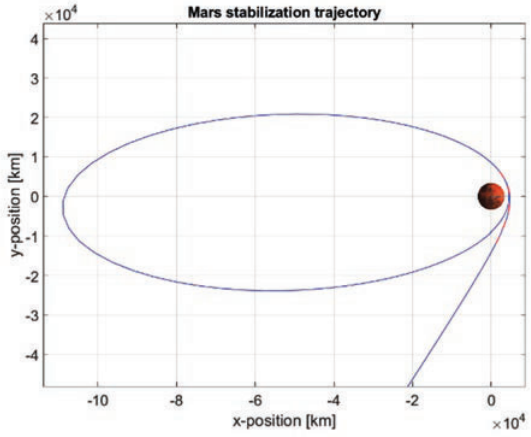

Fig.4 Mars stabilization trajectory.

To stabilize around Mars, the spacecraft shall reduce its orbital speed in order to change the shape of the hyperbolic trajectory to an elliptical one. The spacecraft enters the sphere of influence of Mars following an orbit characterized by a specific energy of $E_{\infty E}$ and, assuming an orbit periapsis of 5,000 km, with an initial hyperbolic orbit eccentricity of 1.8185. For the braking phase, it is assumed that the spacecraft can use the thrusters to propel itself in the opposite direction of its orbital velocity. The trajectory of the spacecraft is simulated by solving the two-body orbital equation of motion around Mars, described by Equation (4):

$$\ddot{\vec{r}} = -\frac{\mu_M}{\left|\left|\vec{r}\right|\right|^3}\vec{r} + \frac{\vec{T}}{m} \tag{4}$$

For the Mars stabilization phase, the thrust level is fixed at 6 N, the optimal value obtained from the Earth escape analysis: having the maximum available thrust provides higher performances, thus the same thrust level is adopted for the stabilization manoeuvres around Mars. In this phase, orbital manoeuvres will last for t_{burn} each, spaced in time by $\Delta t_{burn} = t_{burn}$, similarly to the second phase of Earth escape. The variables considered for the optimization are two: the manoeuvre burn time t_{burn} still limited to a maximum of 600 s, and the true anomaly of the manoeuvre start θ_{man_M}. For this strategy, a value for the true anomaly needs to be found in combination with burn time, obtaining an optimal start point and timing for the braking strategy of the spacecraft around Mars that minimizes the required ΔV. Figure 3 shows the results obtained for an initial spacecraft mass of 28 kg, minus the mass of propellant expelled in the Earth escape phase, with specific impulse of 262.86 s. In red, the combination of θ_{man_M} – t_{burn} for which the mission requirements are not satisfied. The optimal value is found for a manoeuvre burn time of t_{burn} = 526.3 s and a true anomaly of manoeuvre start of θ_{man_M} = 275.7°. The ΔV required for this phase is 956.61 m/s. Figure 4 shows the trajectory followed by the satellite when stabilizing around Mars. Table 4 on the next page shows the complete set of results for the Mars stabilization phase.

The ΔV budget of mission requirement PROP-01 is found by summing up the ΔV budgets required for Earth escape and Mars stabilization phases, accounting for a 10% margin: this leads to a total ΔV budget for the mission of 2,046.34 m/s.

4 PROPULSION SYSTEM AND PROPELLANT TRADE-OFF

4.1 Propulsion system trade-off

Chemical propulsion systems exploit the chemical energy stored in a propellant in order to generate thrust. There exist

TABLE 4: Mars stabilization results

Property	Value	Unit
Initial spacecraft mass	19.7225	kg
Stabilization manoeuvres	5	-
Thrust	6	N
Specific impulse	262.86	s
Manoeuvre burn time t_{burn}	526.3	s
Total burn time	2,627.1	s
True anomaly of stabilization phase start	275.7	deg
Final specific orbit energy	-0.377	km^2/s^2
Final specific orbit eccentricity	0.9196	-
ΔV – Mars stabilization	956.61	m/s
Propellant mass used	6.1127	kg
Minimum distance from Mars	1,180.6	km
Time elapsed after entering Mars' sphere of influence	59.76	h

three main families of chemical propulsion systems: cold gas, solid and liquid. For the context of this work, the cold gas option is not analysed since it does not comply to the thrust and specific impulse levels required for this CubeSat mission. In the next sections, a trade-off between the chemical propulsion system kind to be adopted is performed, followed by the choice of propellant that better meets the scope of this study.

4.1.1 Solid propulsion systems

Solid rocket motors are characterized by relatively low specific impulse values and very high thrust levels. Their low performance in terms of specific impulse I_{sp} and the non-availability of start-stop capabilities does not make solid propulsion systems a consistent choice for this application, in which each propellant burn shall be precisely tuned for every manoeuvre.

4.1.2 Liquid propulsion systems

CubeSat liquid propulsion system, mainly including mono- and bi- propellant systems depending on the number of propellants adopted, are being highly researched by several companies and institutions. For mono-propellant options, the usage of hydrazine which has been the most historic mono-propellant choice in space is seeing less interest due to its high toxicity levels. More interest has grown towards green propellants, needing fewer requirements for safety handling and operation. There are two main propellant families that are the most representative cases of green mono-propellant options: they are either based on ADN (Ammonium dinitramide) or HAN (Hydroxylammonium nitrate).

ADN propellant blends development has started at the Swedish Defence Research Agency (FOI): the main propellant blends are the FLP family, and LMP-103S. The FLP family consists of FLP-103, FLP-105, FLP-106 and FLP-107 while LMP-103S has been developed by Bradford ECAPS. Each of these propellants blends ADN with water and either Methanol or MMF (monomethyl-formamide). They can provide theoretical specific impulse values of around 250 s, while their density varies from 1,310 to 1,405 kg/m^3 [5], leading to very high levels of volumetric specific impulse ρI_{sp} with respect to previous alternatives such as hydrazine. The MARIO mission proposed to choose FLP-106 for its mono-propellant system [3].

Bradford ECAPS has developed a series of LMP103S based thrusters named "HPGP", which provide thrust levels from 0.1 N to 22 N, with specific impulse levels ranging from 196 s to 255 s [6]. One of these thrusters has flight heritage, having two thrusters adopted for the mission PRISMA [7][8].

The most mature HAN-based propellant blend is known as AF-M315E (recently named ASCENT) which was invented at the US Air Force Research Laboratory (AFRL) in 1998. It can deliver around 50% higher volumetric specific impulse than hydrazine, it poses no health hazard and offers performances comparable to traditional bi-propellant systems [9]. Its theoretical specific impulse level is 266 s, while its density is 1,470 kg/m^3 [10]. State-of-the-art mono-propellant thrusters that use HAN-blend propellants have a range of thrust that mostly varies between 0.1 N to 1 N: Aerojet Rocketdyne "MPS" thrusters adopting AF-M315E provide up to 230 s of specific impulse and up to 1 N of thrust [11] , while Busek's BGT-X5 provides 0.5 N of thrust [12]. The NASA Green Propulsion Infusion Mission (GPIM) employed a set of thrusters also developed by Aerojet Rocketdyne named GR-1 using AF-M315E, providing up to 1.4 N of thrust [13]. Another interesting HAN-based mono-propellant is the SHP-163 which has been developed by ISAS (Institute of Space and Astronautical Science) and JAXA: it consists of a blend of HAN, methanol, water and AN (ammonium nitrate) [14]. Compared to the other green propellants listed, it shows the highest adiabatic flame temperature level.

A bi-propellant liquid propulsion system adopts two different propellants, stored in their liquid phase, in order to generate thrust. The two propellants, usually taking the parts of oxidizer and fuel, are injected together in the combustion chamber and by reacting with each other they generate very high temperature levels, causing the reactant gases to be highly accelerated in the nozzle in order to generate thrust. System-wise, bi-propellant propulsion systems need to use at least double of the amount of system tanks and feed lines, since both the propellants need to be stored in their liquid phase and at correct pressurization levels. The benefit of using a bi-propellant system is the higher I_{sp} that they provide with respect to all the other chemical propulsion options. The drawbacks come from the low maturity that such systems have with respect to CubeSat applications, since they are the most complex type of chemical propulsion system based on the number of tanks, feeding lines and possibly pumps to be used, taking up most of the allowable volume. The state-of-the-art options found for bi-propellant systems adapted to CubeSats are manufactured by AAC Clyde Space and Dawn Aerospace, the PM200 [15], and Tethers Unlimited "HYDROS-M" and "HYDROS-C" [16]. The PM200 adopts nitrous oxide and propane, achieving a specific impulse of around 285 s, while the HYDROS family utilizes electrolyzed liquid water, reaching a specific impulse value of 310 s.

4.1.3 Propulsion system choice

To determine which kind of propulsion system better meets the needs of this study, a high-level trade-off has been performed between a solid, mono-propellant and bi-propellant system. Four different high-level criteria have been considered: thrust and specific impulse, the two parameters that have been con-

TABLE 5: High-level propulsion system trade-off

Criteria/choices	Thrust	Specific Impulse	Complexity	TRL
Solid	**Bad** (over 37 N)	Bad (< 240 s)	Good simplest system	Good 9
Mono-propellant	**Good** (0.1-22 N)	OK (> 240 s)	OK easier to manage with single propellant	Good 6-9, with increasing trends
Bi-propellant	**Good** (0.5-1.2 N)	**Good** (> 280 s)	Bad most complicated system	OK < 6

Meets requirement: 2 points Workable solution: 1 point Least preferable: 0 points

sidered in the trajectory analysis phase; they are the main performance parameters of a propulsion system, and intrinsically account for the time to reach the final destination, a key factor of the research. The third parameter is system complexity, which considers the amount of components to be implemented and the proneness to failure. The last parameter considered is Technology Readiness Level (TRL), which takes into account the heritage of the propulsion system choice. Other parameters such as cost, volume, power and thermal management requirements have not been considered at this stage, being a high-level trade-off for a feasibility study.

Each parameter is given a score from 0 to 2, from "not meeting" requirement to "satisfying" requirement. The result of the trade-off is shown in Table 5 and scores 4 points for the solid option, 6 for the mono-propellant and 5 for the bi-propellant. A sensitivity analysis is performed on the weight of the "workable solution" between 0.5 and 1.5, while keeping the other two weights at 0 and 2 respectively, and the trade-off is still favourable to a mono-propellant system, proving the robustness of the choice. Therefore, a mono-propellant system design will be explored for the rest of the research.

4.2 Propellant option trade-off

The two main green propellant options available at this current stage are either derived from ADN or HAN. These two energetic ionic liquids (EIL) are salts characterized by high internal nitrogen and oxygen contents, which make them highly energetic. The rest of the section focuses on the detailed description of the chemical composition of both the available ADN- and HAN-type blends currently available or in development for miniaturized propulsion systems.

4.2.1 ADN-based propellants

ADN stands for ammonium dinitramide and is a colourless salt with high solubility in water. Its chemical formulation is $[NH_4]^+[N(NO_2)_2]^-$. Contrary to the HAN-counterparts, ADN-based propellants can not only be ignited by adopting a preheated catalytic bed but also by using thermal ignition, either pyrotechnic or resistive, reducing the amount of power needed to operate the thruster [17].

4.2.2 HAN-based propellants

HAN stands for hydroxylammonium nitrate, chemical composition $[NH_3+OH]^+[NO_3]^-$, and is a salt of the nonstable base hydroxylamine and nitric acid. Due to the polar character of the HAN molecule, the solubility in water or other solvents is sufficient to form liquid propellants, making technical handling like pumping more feasible. The addition of fuels and water gives the opportunity of changing the propellants' enthalpy, adiabatic combustion temperature and physical-chemical properties, just like for ADN-blends [18]. AF-M315E (which stands for Air Force Mono-propellant 315E) represents the state-of-the-art for HAN-based mono-propellants: it has also been flown on the GPIM (Green Propellant Infusion Mission) with thrusters developed by Aerojet Rocketdyne. It consists of a mixture of HAN, HEHN (hydroxyethyl-hydrazinium nitrate) and water.

4.2.3 Propellant choice

All the propellant candidates show several improvements with respect to the hydrazine option: density is considerably higher, as well as the specific impulse, which causes the volumetric specific impulse to be even higher. Most importantly, the acute toxicity value is considerably lower, which improves the greenness of the propellant. The vapour pressure values are similar, while the combustion temperatures are higher as predicted: ADN- and HAN-based propellants are very energetic and therefore release much more enthalpy in the combustion chamber, which translates into higher performance values, at the cost of higher combustion temperatures. Nevertheless, the values for specific and volumetric specific impulse are increased, which means that performance and compactness can be improved by adopting one of these propellant candidates for an interplanetary Mars CubeSat mission.

Propellant physical and chemical parameters are found in Table 6. Chemical compositions are found in [19]: adopting the RPA (Rocket Propulsion Analysis) tool, together with equations from ideal rocket theory, the performance parameters are simulated for a nozzle expansion ratio up to 200.

Thanks to the better performance in terms of both specific impulse and lower volume requirement, the propellant choice for this feasibility study is AF-M315E (ASCENT). Theoretically, it can provide an ideal specific impulse in vacuum of I_{sp} = 266 s (at a chamber pressure of 2 MPa and nozzle expansion ratio of 50 [10]), with a density of 1,470 kg/m^3, resulting in the highest theoretical volumetric specific impulse between all the candidates of ρI_{sp} = 391 kg*s/dm^3 at the cost of a very high

TABLE 6: Physical, performance and thermochemical properties of the propellant candidates*

Property [unit]	SHP163	AF-M315E	FLP-106	LMP-103S
Density [kg/dm^3]	1.4 [14] , 1.411 [36]	1.47 [10], 1.5 [14]	1.357 [36],[38]	1.238 [39], 1.24 [10]
Specific impulse [s]	276a [14],[35]	266b [10]	255b [36], 261 b [40]	252b[19]
Volumetric specific impulse [kg/dm^3]	386 [35]	390 [14]	354 [26]	312
Flame temperature [K]	2,401 [14], 2,373 [35]	2,166 [14]	2,095 [36]	1,903 [19]
Freezing temperature [K]	<-30 [14], <-37 [35]	<-22 [14]	0 [40]	-7 [40]
Dynamic viscosity @25°C [mPa•s = cP]	11.9 [35]	25 [41], 27 [42]	3.7 [36][38]	3 [39]
Vapour pressure [mbar]	-	14 [10]	<21 [38]	136 [39]
Acute toxicity LD_{50} oral, dermal [mg/kg]	300-2,000, >2,000 [14]	Moderate [10]	1270, - [40]	750-800, - [40]
Heritage	RAPIS-1 [14]	GPIM [37]	-	PRISMA [8]

*Conditions for specific impulse estimation: a) Pc=0.7 MPa, $A_e/A_t = 50$, b) Pc = 2 MPa, $A_e/A_t = 50$

flame temperature of 2,166 K. Considering a specific heat ratio of 1.21 [20], a total combustion and nozzle efficiency of 0.9445 combined (obtained with the RPA tool) the real expected specific impulse level is 262.86 s, for an expansion ratio of 200.

5 PROPULSION SYSTEM DESIGN

5.1 Baseline thruster configuration

Looking at the state-of-the-art thrusters, Busek Inc. and Aerojet Rocketdyne both employ AF-M315E as propellant: the first has developed the BGT-X5, a class 0.5 N thruster, while the latter has developed two different class thrusters of 1 and 22 N, respectively GR-1 and GR-22. The thrust level of the propulsion system has been fixed at the value of 6 N, obtained by mission analysis, therefore it is decided to design the thruster based on the Aerojet Rocketdyne thruster GR-1. A set of these thrusters adopting AF-M315E has already been used for the GPIM mission for NASA [21]: each of these thrusters has the capability of generating a thrust of 1 N nominally, but this value can increase based on the higher the feed pressure is, as can be noted from Table 7.

Given the requirement of a total thrust level of 6 N, it is decided to adopt five thrusters in total: four at the corners of a square and one positioned in the centre. Each thruster will be sized to provide up to 1.2 N of thrust, to match the requirement of 6 N.

As per the chamber pressure value, no data is available from the GR-1 data sheet. Since the specific impulse value for the AF-M315E propellant has been obtained by using ideal rocket theory starting from the literature value of chamber pressure of 2 MPa, the same value shall be adopted for chamber design. To be consistent with the current state-of-the-art thruster GR-1, a feed pressure of 32 bar is adopted for the feed system design.

5.2 Pressurization system

The pressurization system choice is critical, since a high volume of propellant needs to be carried on board. This means that a blow-down system would not be preferable due to the high amount of pressurant volume to be carried. The same applies to a regulated pressure system in which a highly pressurized gas needs to be used. Therefore, it is decided to provide the design feed pressure combining an initial smaller pressurization of the tank, in blow-down mode, with the pressure differential provided by a pump; an initial pressurization of the tank at 1.2 MPa is applied, while the pump will provide the pressure differential to match the feed pressure. This component shall work at different operating points throughout the mission, with the most critical one being at the end of the mission when the pressurizing gas has expanded and the highest pressure differential shall be delivered by the pump. The option of using a pump for a CubeSat propulsion system is becoming more popular, as it allows for higher feed pressure levels at the cost of additional power, but with reduced volume impact since components are becoming smaller and can fit inside a CubeSat. Recent proposals of this application to CubeSat missions are found in [22] [23]. The component that better fits the needs of the propulsion system requirement is found in [24]: it can provide up to 30.3 bars of pressure differential for a volumetric mass flow of 95 mL/min, coherently with the requirements of the propulsion system at worst case. The expected power requirement is of 35 W at these conditions. The mass of the pump is 175 g, having a total length of 99.2 mm and a diameter of 22 mm.

TABLE 7: Feed pressure - Thrust for GR-1 thruster [9]

Property	Value	Unit
Feed pressure	37.9-6.9	bar
Thrust	1.42-0.26	N

The tank has been sized to withstand a pressure of 1.75 MPa, with a margin on the design pressurization value. Different shapes have been investigated: a particular interest has been put towards the option of adopting a prismatic shaped tank, which would minimize the volume intake by using all the available CubeSat section. This comes at the cost of very high thickness levels to sustain the initial pressurization, leading up to a tank mass of over 20 kg, when adopting Ti-6Al-4V. The choice of a cylindrical shaped tank with hemi-spherical caps is still better in terms of mass, even if it occupies more of the available volume of the 24U CubeSat. The latter is the choice for the mission, made from Ti-6Al-4V. Tank design details are presented in Table 8.

5.3 Chamber and thruster design

5.3.1 Catalyst bed

For the correct decomposition of a mono-propellant, a catalyst bed is employed: typical catalyst beds can be either monolithic or granulated, with the latter choice being the most

TABLE 8: Tank, propellant and pressurant volume and mass

Property	Value	Unit
Propellant volume	10.433	dm^3
Propellant density	1.47	kg/dm^3
Propellant mass	15.337	kg
Pressurant volume (GN_2)	1.742	dm^3
Pressurant density @298K	15.866	kg/m^3
Pressurant mass	0.028	kg
PMD volume	0.564	dm^3
Tank internal radius	98	mm
Tank thickness (circumference)	0.29	mm
Tank thickness (cap)	0.146	mm
Tank total height	486.47	mm
Tank density (Ti-6Al-4V)	4.430	kg/dm^3
Tank mass	0.31	kg

TABLE 9: Thruster and chamber dimensions and mass

Property	Value	Unit
Throat diameter	0.64	mm
Exit area ratio	200	-
Nozzle exit diameter	9.04	mm
Contraction ratio	96.63	-
Chamber diameter	6.285	mm
Characteristic length	1.5	m
Chamber volume	481.578	mm^3
Contraction angle	30	deg
Chamber contraction length	4.889	mm
Total chamber length	18.6	mm
Nozzle expansion half angle	15	deg
Chamber + nozzle combined length	34.32	mm
Estimated single thruster mass (without valves) [33]	200	g

common. To preliminary design the catalyst bed pellets in dimensions, a model from Bey and Eigenberger [25], revised in [26], has been adopted. It allows for an initial pellet dimension estimation with respect to total catalyst bed diameter: a cylindrical pellet with small diameter would provide low variations in catalyst bed void fraction, leading to correct propellant reaction by not creating preferrable paths for the propellant in the chamber. On the other hand, with smaller pellet diameters the pressure drop along the catalyst bed increases significantly. The suggested value for the bed-to-pellet diameter ratio for this application is fixed at 7.

Based on state-of-the-art mono-propellant thruster employing hydrogen peroxide or hydrazine [27], a catalyst bed loading factor of 20 $kg/m^2/s$ is chosen, obtaining the catalyst bed (and chamber) diameter of 6.285 mm. The diameter and length of the cylindrical shaped pellets for the catalyst bed are fixed to 0.8978 mm, using the bed-to-pellet diameter ratio of 7.

The catalyst bed material is chosen based on current research: in recent years, several laboratory tests have been performed in order to verify the capabilities of catalytic decomposition of AF-M315E. The GPIM mission, adopting the GR-1 thrusters on which this design is based off, adopted the LCH-240 catalyst [28]. This catalyst composition from Aerojet Rocketdyne, together with the models LCH-240(A) and LCH-241, has proved to withstand the high temperatures of AF-M315E decomposition and to satisfy of a total run time of 11.5 hours total [29]. The GR-1 maximum continuous burn time is of 20 minutes [30], on the same order of magnitude of the 10 minutes burn time t_{burn} adopted in the preliminary mission analysis, thus the same material is adopted for this preliminary catalyst bed sizing. The LCH-240 catalyst is made from cylindrical catalyst pellets of hafnium oxide with 5% iridium: the granules range from values of 0.025 in (0.635 mm) up to 0.050 in (1.27 mm) [31]. These dimensions fit the preliminary design dimensions of the catalyst pellets length and diameter obtained by assuming a bed-to-pellet diameter ratio of 7, therefore the composition of hafnium oxide with 5% iridium is suggested as the pellet material. The GR-1 thruster requires 10 W of catalyst bed preheat power due to the high temperatures at which the AF-M315E starts the decomposition process: in latest researches, the development of a successor of the GR-1 thruster named "GR-1A" has brought light on the possibility of reducing this value by 30% [28], hence requiring a preheat power of 7 W. The latter value will be used for the preheat power requirement of the catalyst bed.

5.3.2 Thruster design

A chamber temperature of 2,166 K is very high compared to other mono-propellant flame temperatures: the material employed for the chamber and thruster design is rhenium. It has a density of 20,800 kg/m^3 and a yield strength of 290 MPa [32]. The throat area of the thruster is found with Equation (5):

$$A_t = \dot{m}\frac{\sqrt{RT_c}}{\Gamma P_c} \tag{5}$$

Fixing the contraction area ratio and half angle, as well as the exit area ratio and expansion half angle, the geometry of the thruster is constrained. Thruster design values, obtained by catalyst bed design and thermo-chemical properties of AF-M315E are shown in Table 9.

5.4 Propulsion system architecture and budgets

Given all the previous considerations, a schematic of the propulsion system architecture is shown in Figure 5.

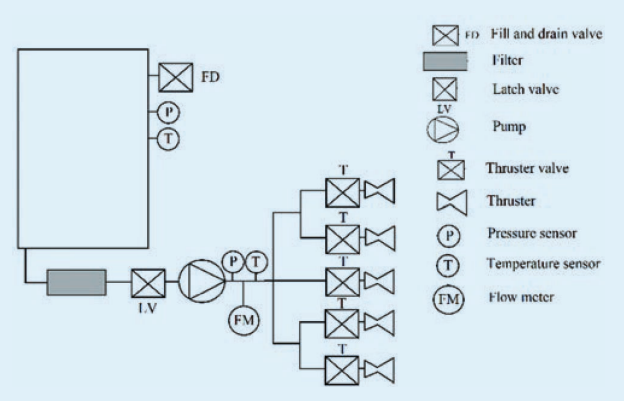

Fig.5 Propulsion system architecture.

TABLE 10: Propulsion system mass

Component	Material/Part	Mass [g]
Tank	Ti-6Al-4V	310
Pump	FlightWorks Inc. 2212-M04X01	175
Filter	VACCO F1D1080702	25
Latch valve	VACCO V8E1058001	160
Thruster valve (x5)	VACCO V0D1089801	425
Tubing	Swagelok SS-T4-S-065-6ME	100.7
Thrusters (x5)	Rhenium	1,000
Total dry mass	only considering main components	2,195.7
Total dry mass (margined 5%)	only considering main components	2,305.49
Pressurant mass	GN_2	28
Propellant mass	AF-M315E (ASCENT)	15,337
Propulsion system wet mass	-	17,670
Mass budget	Payload and subsystems	10,330

The main components that have been added are a fill-and-drain valve for the tank, together with a pressure and a temperature sensor. Before the pump, a latch valve has been implemented; after the pump, a flowmeter, a pressure and a temperature sensor have been added, in order to check the operating point of the pump. Finally, the feeding lines are split into five lines, each comprising of a thruster valve and injector, leading the propellant inside the thrust chamber.

5.5 PROPULSION SYSTEM MASS, VOLUME AND POWER BUDGET

The mass budget comprises all dry components, propellant and pressurant: Table 10 presents the overall mass budget. The dry mass is considered as the sum of all inert components' masses. A margin is added to the dry mass only, since the propellant mass has already been increased when adding a margin on the total ΔV budget of the mission. Propellant and pressurant masses are added to obtain the propulsion system wet mass, and the available mass budget for the mission is obtained by considering an initial spacecraft mass of 28 kg: this leaves 10.3 kg available for the rest of the subsystems and payloads on-board.

Carrying a very high mass of propellant considerably limits the availability of volume that can be reserved for the rest of CubeSat subsystems and payloads. The total height of the tank is 486 mm, occupying over 19 U of a 24 U CubeSat. Accounting for the rest of the propulsion system feeding lines and components, an additional 40 mm are needed, bringing the total height of the propulsion system to 526 mm, occupying a volume of 21 U and leaving 3U for the other subsystems and payloads. The CAD model representing the propulsion system is highlighted in Appendix A.

The power budget is shown in Table 11, considering the peak power required when thrusting, which comprises the activation of the pump, latch valve and all five thruster valves together. The catalyst bed heaters are active only before thrusting and are not accounted in the peak power budget.

6 CONCLUSIONS

The amount of propellant required for a deep-space mission to Mars highly constrains the volume and mass left available for the other subsystems, due to the high ΔV requirement of such a mission. Compared to electrical propulsion system, the mass and volume occupied are much higher due to the low specific impulse I_{sp} of chemical propellants when compared to their electric counterparts. On the other hand, the availability of high levels of thrust allows for the reduction of travel time to 301.8 days, while it amounts to years when looking at electric-propelled deep-space missions. The total peak power budget of the system hereby presented amounts to 83 W, lower than the 111 W budget for MARIO [34], even though several feed system components and thrusters have been included in the design. Due to volume limitations, adopting a pump-fed system in order to reduce the impact of pressurization increases the power burden on the system, but leaves more flexibility for the allocation of the rest of the subsystems and payload. The volume budget left considering a 24U CubeSat is around 3U: if the components are arranged more efficiently, it is believed that more volume budget can be available to the rest of subsystems and payloads. Even better results can be expected for interplanetary missions requiring slightly lower ΔV budgets, such as Near Earth Objects exploration or asteroid flyby missions.

TABLE 11: Propulsion system peak power requirement

Component	Part	Power [W]
Pump	FlightWorks Inc. 2212-M04X01	35.12 (max)
Latch valve	VACCO V8E1058001	28 (max)
Thruster valve (x5)	VACCO V0D1089801	20 (max)
Catalyst bed heater (x5)	assuming GR-1A configuration	35
Peak power when thrusting	catalyst bed heaters are turned off when thrusting	83.12 (max)

APPENDIX A – CAD MODEL

In this Appendix, images from the CAD model of the propulsion system are presented. The images are to scale, including all components listed in Table 10.

REFERENCES

1. Schoolcraft, J., Klesh, A., and Werne, T. (2017). "MarCO: interplanetary mission development on a CubeSat scale". In *Space Operations: Contributions from the Global Community* (pp. 221-231). Springer, Cham.
2. Speretta, S., Cervone, A., Sundaramoorthy, P., Noomen, R., Mestry, S., Cipriano, A., and Walker, R. (2019). "LUMIO: an autonomous CubeSat for lunar exploration". In *Space Operations: Inspiring Humankind's Future* (pp. 103-134). Springer, Cham.
3. Mani, K. V., Casado, A. S., Franzese, V., Cervone, A., and Topputo, F. (2019, October). "Systems Design of MARIO: Stand-alone 16U CubeSat from Earth to Mars". In *70th International Astronautical Congress, Washington DC* (pp. 1-17).
4. SpaceX Space Launch Report – Falcon 9: https://sma.nasa.gov/LaunchVehicle/assets/spacex-falcon-9-v1.2-data-sheet.pdf [Last visited 31 March 2023]
5. Wingborg, N., Eldsäter, C., and Skifs, H. (2004, October). "Formulation and characterization of ADN-based liquid mono-propellants". In ESA Special Publication (Vol. 557)
6. Bradford ECAPS. "Ecaps hpgp thrusters". https://www.ecaps.space/products-overview-ecaps.php [Accessed 17 September 2021]
7. Persson, S., Veldman, S., and Bodin, P. (2009). PRISMA – A Formation Flying Project in Implementation Phase. *Acta Astronautica*, **65**(9-10), 1360-1374.
8. Anflo, K., and Crowe, B. (2011, July). "In-space Demonstration of an ADN-based Propulsion System". In 47th *AIAA/ASME/SAE/ASEE Joint Propulsion Conference & Exhibit* (p. 5832).
9. Spores, R. A. (2015). "GPIM AF-M315E propulsion system". In *51st AIAA/SAE/ASEE Joint Propulsion Conference* (p. 3753).
10. Thrasher, J., Williams, S., Takahashi, P., and Sousa, J. (2016). "Pulsed Plasma Thruster Development Using A Novel HAN-Based Green Electric Mono-propellant". In *52nd AIAA/SAE/ASEE Joint Propulsion Conference* (p. 4846).
11. Aerojet Rocketdyne. Modular Propulsion Systems Data Sheet. https://www.rocket.com [Accessed 2 December 2019]
12. Busek. "Green mono-propellant thruster bgt-x5". https://www.busek.com/bgtx5 [Accessed 17 September 2021]
13. Masse, R., Allen, M., Spores, R., and Driscoll, E. A. (2016). "Af-m315e Propulsion System Advances and Improvements. In *52nd AIAA/SAE/ASEE Joint Propulsion Conference* (p. 4577).
14. Hori, K., Katsumi, T., Sawai, S., Azuma, N., Hatai, K., and Nakatsuka, J. (2019). "HAN-Based Green Propellant, SHP163 – Its R&D and Test in Space". *Propellants, Explosives, Pyrotechnics* **44**(9), 1080-1083.
15. AAC Clyde Space. Pm200 data sheet. https://www.aac-clyde.space/wp-content/uploads/2021/11/PM200.pdf [Accessed 31 August 2022]
16. Tethers Unlimited. Hydros data sheet. https://www.tethers.com/wp-content/uploads/2019/09/2019-HYDROS.pdf [Accessed 14 October 2021]
17. Wingborg, N., Larsson, A., Elfsberg, M., and Appelgren, P. (2005, July). "Characterization and Ignition of ADN-based Liquid Mono-propellants". In 4*1st AIAA/ASME/SAE/ASEE Joint Propulsion Conference & Exhibit* (p. 4468).
18. Freudenmann, D., and Ciezki, H. K. (2019). "ADN and HAN-Based Mono-propellants – a Mini-review on Compatibility and Chemical Stability in Aqueous Media". *Propellants, Explosives, Pyrotechnics*, **44**(9), 1084-1089.
19. Nosseir, A. E., Cervone, A., and Pasini, A. (2021). "Review of State-of-the-art Green Mono-propellants: for Propulsion Systems Analysts and Designers. *Aerospace*, **8**(1), 20.
20. McGee, A. (2017). "Hot-Fire Testing of an AF-M315E 1-Newton Thruster ", master's thesis available at https://egrove.olemiss.edu/hon_thesis/19/
21. McLean, C. H. (2020). Green Propellant Infusion Mission: Program Construct, Technology Development, and Mission Results. In *AIAA Propulsion and Energy 2020 Forum* (p. 3810).
22. Nosseir, A. E., Cervone, A., and Pasini, A. (2021). "Modular Impulsive Green Mono-propellant Propulsion System (mimps-g): for CubeSats in Leo and to the Moon". *Aerospace*, **8**(6), 169.
23. Huggins, G. M., Talaksi, A., Andrews, D., Lightsey, E. G., Cavender, D., McQueen, D., and Kowalkowski, M. (2021). "Development of a CubeSat-Scale Green Mono-propellant Propulsion System for NASA's Lunar Flashlight Mission". In *AIAA Scitech 2021 Forum* (p. 1976).
24. Flightworks Inc. "Mseries (Magnetic drive gear pumps) models 2122 m04x01/x03/x04", https://products.flightworksinc.com/Asset/Product%20Data%20Sheet%20(2212-M04X01.X03.X04).pdf [Accessed 28 November 2021]
25. Bey, O., and Eigenberger, G. (1997). Fluid flow Through Catalyst-filled Tubes. *Chemical Engineering Science,* **52**(8), 1365-1376.
26. Michele Negri, Marius Wilhelm, Christian Hendrich, Niklas Wingborg, Linus Gediminas, Leif Adelöw, Corentin Maleix, Pierre Chabernaud, Rachid Brahmi, Romain Beauchet, et al. "New Technologies for Ammonium Dinitramide Based Mono-propellant Thrusters – the Project Rheform. *Acta Astronautica*, **143**:105-117, 2018.
27. Franken, T., Valencia-Bel, F., Jyoti, B. V. S., and Zandbergen, B. (2020). "Design of a 1-N Mono-propellant Thruster for Testing of New Hydrogen Peroxide Decomposition Technologies". In *Aerospace Europe Conference.*
28. Masse, R. K., Spores, R., and Allen, M. (2020). AF-M315E Advanced Green Propulsion – GPIM and beyond". In *AIAA Propulsion and Energy 2020 Forum* (p. 3517).
29. Masse, R., Overly, J., Allen, M., and Spores, R. (2012). A New State-of-the-art in AF-M315E Thruster Technologies". In *48th AIAA/ASME/*

SAE/ASEE Joint Propulsion Conference & Exhibit (p. 4335).

30. Masse, R. K., Spores, R. A., Allen, M., Kimbrel, S., and McLean, C. (2015). "Enabling High Performance Green Propulsion for SmallSats".
31. Polaha, J. (2011). U.S. Patent Application No. 12/948,558.
32. Berg, S. P., and Rovey, J. L. (2017). Assessment of Multimode Spacecraft Micropropulsion Systems. *Journal of Spacecraft and Rockets*, **54**(3), 592-601.
33. ArianeGroup. Chemical mono-propellant thruster family. https://www.space-propulsion.com/brochures/hydrazine-thrusters/hydrazine-thrusters. [accessed 8 January 2022]
34. Mani, K. V. (2020). "Combined Chemical-electric Propulsion Design and Hybrid Trajectories for Stand-alone Deep-space CubeSats", doctoral thesis available at https://www.politesi.polimi.it/handle/10589/152157
35. Amrousse, R., Katsumi, T., Azuma, N., and Hori, K. (2017). Hydroxylammonium nitrate (HAN)-based Green Propellant as an Alternative Energy Resource for Potential Hydrazine Substitution: From Lab Scale to Pilot Plant Scale-up". *Combustion and Flame*, **176**, 334-348.
36. Wingborg, N., Johansson, M., and Bodin, L. (2006). "Initial Development of a Laboratory Rocket Thruster for ADN-based Liquid Monopropellants". Swedish Defence Research Agency.
37. McLean, C. H. (2020). Green propellant Infusion Mission: Program Construct, Technology Development, and Mission Results. In *AIAA Propulsion and Energy 2020 Forum* (p. 3810).
38. Wurdak, M., Strauss, F., Werling, L., Ciezki, H. K., Greuel, D., Lechler, R., and Scharlemann, C. (2012, May). "Determination of Fluid Properties of the Green Propellant FLP-106 and Related Material and Component Testing with Regard to Applications in Space Missions". In *3rd Space Propulsion Conference, Bordeaux, France* (pp. 1-8).
39. Persson, M., Anflo, K., and Friedhoff, P. (2019). "Flight Heritage of Ammonium Dinitramide (ADN)-based High Performance Green Propulsion (HPGP) Systems". *Propellants. Explosives, Pyrotechnics* **44**(9), 1073-1079.
40. Gohardani, A. S., Stanojev, J., Demairé, A., Anflo, K., Persson, M., Wingborg, N., and Nilsson, C. (2014). "Green space propulsion: Opportunities and Prospects". *Progress in Aerospace Sciences*, **71**, 128-149.
41. Dimas, E., Holland, G., Masse, R., Dawley, S., Brown, N., Holmes, R., and Eck, W. (2019). "Environmentally Sustainable Liquid Gas Generator Formulations Program". Aerojet Rocketdyne, Redmond, United States.
42. Tsay, M., Feng, C., Paritsky, L., Zwahlen, J., Lafko, D., and Robin, M. (2016). "Complete EM System Development for Busek's 1U CubeSat Green Propulsion Module. In *52nd AIAA/SAE/ASEE Joint Propulsion Conference* (p. 4905)

Received 17 February 2023 **Approved** 18 May 2023